Proceedings of the 17th World Congress
The International Federation of Automatic Control
Seoul, Korea, July 6-11, 2008

Design and Implementation of a Visual Feedback Control System Driven by Wires

Akira Shimada * **Kazuyuki Gotoh** **

* *Department of Electrical System Engineering, Polytechnic University, Hashimotodai 4-1-1, Sagamihara-shi, Kanagawa, Japan. (Tel: +81-42-763-9139; e-mail: ashimada@uitec.ac.jp)*
** *Department of Electrical System Engineering, Polytechnic University, Hashimotodai 4-1-1, Sagamihara-shi, Kanagawa, Japan. (Tel: +81-42-763-9139; e-mail: m19507@uitec.ac.jp)*

Abstract: This paper introduces a visual feedback control method for a multiple degree of freedom mechanical system driven by wires. This system is a small serial-link robot. It consists of a small-diameter tube and two pairs of wires, which are connected to the interior of the terminal link, which pass through the interior of every other link. The mechanical system is driven by electrical motors via tension in the wires. One pair of wires is for side-to-side motion while the other pair is for up-and-down motion. Such a mechanism is frequently used in medical and industrial devices, such as endoscopes. Furthermore, a compact CCD camera is mounted on the terminal link and functions as a vision sensor. The control system consists of a visual feedback control loop and a minor loop that directly controls the sum of all the joint angles. The control law of the minor loop is designed based on a Lyapunov's theory. On the other hand, the outer visual feedback control loop is designed to track a target point detected by the vision sensor. Each loop is connected by an image Jacobian number and its inverse, which are continually updated during operations. This control method is evaluated experimentally. It is anticipated that this system will be used in a variety of applications in the future.

1. INTRODUCTION

This paper introduces a visual feedback control method for a multiple degree of freedom mechanical system driven by wires[1, 2]. A great number of technical papers and reports have been published in the field of robotics and various robot control methods based on visual feedback control have been developed and improved[3, 4, 5, 6]. The movement of multiple degree of freedom robots, such as snake robots, on uneven terrain or in tubes has been studied[7, 8]. Some of these robots have free joints that do not have any actuators[9, 10]. Generally, such mechanisms are classified as nonholonomic systems[11, 12].

The system described in this paper is a small serial-link robot with free joints. Each link of the robot consists of small-diameter tube and two pairs of wires, which are connected to the interior of the terminal link, which are in turn pass through the interior of every other link. The mechanical system is driven by electrical motors via tension in the wires. One pair of wires is for side-to-side motion, while the other pair is for up-and-down motion. Such mechanisms are frequently used in medical and industrial devices, such as endoscopes. A typical example of a mechanism with free joints is an inverted pendulum. Recently, investigations of the swing-up control of inverted pendulums have highlighted non-holonomic control. Furthermore, rapid movement control of inverted pendulums has been reported[13]. Manipulators with free joints have also been developed[10] and control methods for multiple degree of freedom robots with free joints have been studied[9]. A characteristic of such control methods is that positioning is performed by swinging the first active joint. The technique we have developed differs from these methods, since the system described in this paper does not have a first active joint. Furthermore, the system is frequently subjected to disturbance forces in the vicinity of the origin. Generally, since systems with free joints are flexible, the impact imparted to them by collisions is very small. Furthermore, they are also able adjust their shape to conform to tube walls. It is thus anticipated that they will be used in a variety new applications[9].

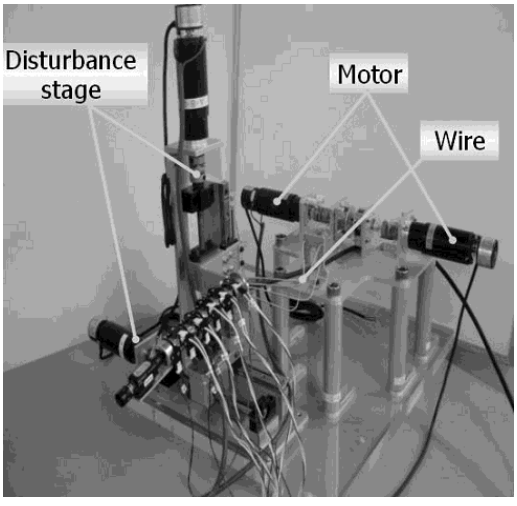

Fig. 1. Overview of the mechanical system

978-1-1234-7890-2/08/$20.00 © 2008 IFAC **10.3182/20080706-5-KR-1001.1855**

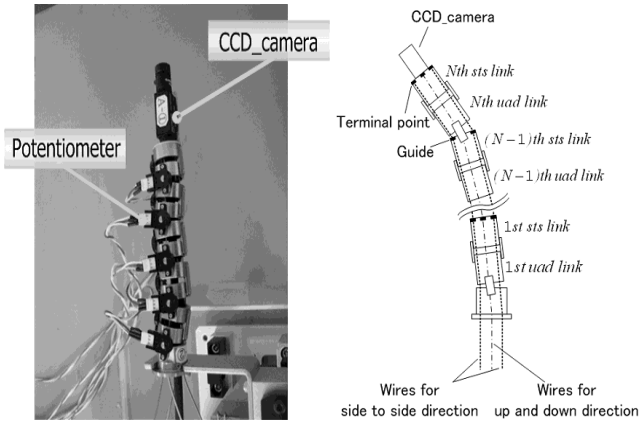

Fig. 2. Close-up photograph and internal structure of the apical section

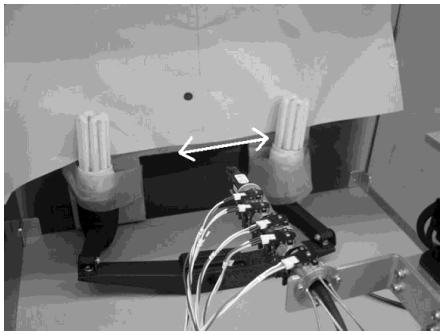

Fig. 3. Side-to-side motion

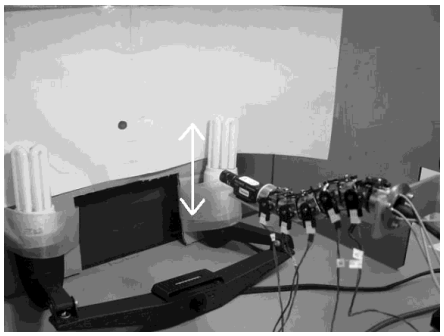

Fig. 4. Up-and-down motion

The aim of this paper is to introduce a visual feedback control method for the above-mentioned system. A compact CCD camera is mounted on the terminal link and functions as a vision sensor for an active vision sensor system. Such systems are frequently employed in medical and industrial endoscopes. Operators of endoscopes need to be experienced technicians and they control endoscopes manually. Therefore, any automatic control method must have the potential to assist endoscope operators. Thus, we present a controller that implements this basic aim. The controller consists of a minor loop and an outer loop. The control law of the minor loop is based on Lyapunov's stability theory and it directly controls the sum of all the joint angles. The outer visual feedback control loop is designed to track a target point detected by the vision sensor. Each loop is connected by an image Jacobian number and its inverse, which are continually updated during operations.

Finally, this control method is evaluated experimentally.

2. MECHANICAL STRUCTURE

The mechanical system is a small serial-link robot. The N joints for side-to-side motion and the N joints for up-and-down motion are allocated interchangeably from the base to the terminal. The total number of joints is thus $2N$, where N is a natural number. In this paper, N is taken to be five. All the joints are free joints, and their angles are measured by potentiometers. There are air holes inside all the links and two pairs of wires are connected to the interior of the terminal link, which passes through the interior of every other link. The system is driven by electrical motors via tension in the wires. One pair of wires is for side-to-side motion while the other is for up-and-down motion. We assume that the side-to-side and up-and-down motions are decoupled from each other, so that the controllers for both types of motion can be designed independently. Fig.1 shows a photograph of a prototype of the mechanical system. The extension in the lower left of the figure is the mechanical serial-link consisting of free joints connected to each other. A compact CCD camera is mounted on the terminal link. An electrical motor for side-to-side motion and another motor for up-and-down motion are mounted. The base of the system is mounted on a two-degree-of-freedom disturbance stage, which introduces positional disturbances for evaluating the motion control performance. Fig.2 shows a close-up photograph and internal structure of the free joint section. Ten links are connected in series. Furthermore, Fig.3 shows a typical side-to-side motion of the system and Fig.4 shows a typical up-and-down motion.

3. KINEMATICS AND DYNAMICS

3.1 Kinematics and Image Jacobian Matrix

When the angles of all of the joints are 0 rad, the above-described mechanical system is horizontally level. The center of the first joint is defined as the origin. The direction of the terminal is defined as the ${}^bX$ axis and the axis in the upper vertical direction is defined as the ${}^bZ$ axis. The direction of the ${}^bY$ axis is obtained by rotating the ${}^bX$ axis about the ${}^bZ$ axis by $\pi/2$rad. Consequently, the Σ_b coordinate frame is defined by the ${}^bX, {}^bY and {}^bZ$ axes. With the exception of gravity, there is no difference between the side-to-side motion and the up-and-down motion. We therefore use the same characters to represent the physical parameters for both motions, except for special cases.

Next, we define the joint-angle vector $\theta = [\theta_1, \theta_2, \theta_3, \cdots, \theta_N]^T$. For both the side-to-side direction and the up-and-down direction, the sum of joint angles $\theta_{sum} = \sum_{i=1}^{N} \theta_i$ is equal to the orientation of the terminal link in the base coordinate system Σ_b. Fig.5 illustrates the relationship between the joint angles and the position of the target point on the screen. In this figure, the origin of the camera coordinate system Σ_c is defined as the center of the CCD camera. We assume that the sum of angles in the left and right figures are equal. But, the positions of the Nth link (i.e., the positions of the CCD camera) are different in Σ_b. It should be noted that the positions of center points of the screens differ somewhat. Here, the relationship between the minimal change of the sum of angles θ_{sum} and the minimal change of the CCD camera position is expressed

by the Jacobian matrix J_{sum}. Further, the relationship between the minimal change of the CCD camera position for a quiescent point and the position of the target point on the screen is expressed by the Jacobian matrix J_{camera}, where $J_{image} = J_{camera} \cdot J_{sum}$.

Fig.6 illustrates the relationship between the transverse component (u) of the position of the target point in the moving camera coordinate system Σ_c that is centered on the actual CCD camera. A virtual screen is then defined, being located at a distance equal to the virtual focal length f from the origin of Σ_c. And $u_T = u - u_0$ in the figure. The figure shows only the u direction; the v direction is defined in the same manner. For the transverse component, the equation ${}^c x_T / {}^c z_T = s_x / f \cdot u_T$ holds, where s_x is the scale ratio ($m/pixel$). J_{camera} is a function of ${}^c z$ and the virtual screen coordinate of the target point, and it is expressed by Eq.(1) [6]D

$$\begin{aligned} \dot{u}_T &= [\frac{-f}{s_x {}^c z_T}, \frac{u_T}{{}^c z_T}, -(\frac{f}{s_x} + \frac{s_x}{f} \cdot u_T^2)] \cdot [{}^c\dot{x}, {}^c\dot{z}, {}^c\omega_y]^T \\ &= J_{camera} \cdot {}^c\dot{X} \end{aligned} \tag{1}$$

Next, J_{sum} is generally expressed by Eq.(2). The first and second components $f(\theta), g(\theta)$ are functions of the joint angles. Even if the different minimal changes of $\dot{\theta}_{sum}$ are equal to each other, the values of $\theta_1 \cdots \theta_N$ may differ, and then ${}^c\dot{x}, {}^c\dot{z}$ will also be different. However, the third component will be unity since ${}^c\omega_y = \dot{\theta}_{sum}$.

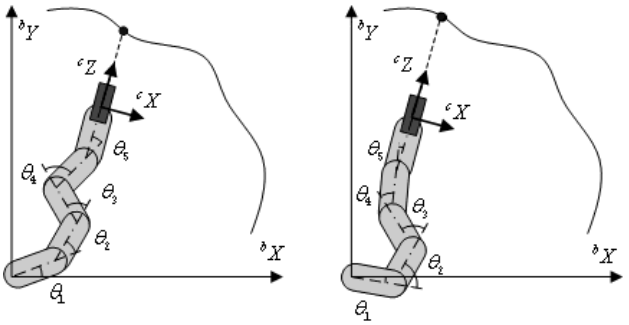

Fig. 5. Relationship between the target point and angles

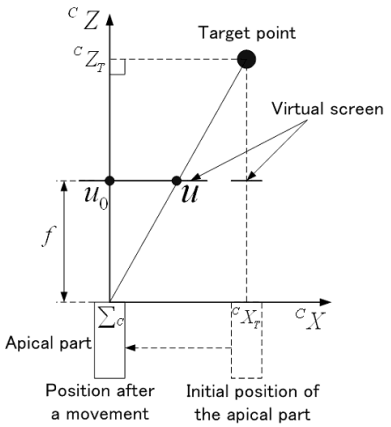

Fig. 6. Before and after views of side-to-side motion in the camera coordinate system and visual screen

$$ {}^c\dot{X} = [f(\theta), g(\theta), 1]^T \cdot \dot{\theta}_{sum} = J_{sum} \cdot \dot{\theta}_{sum} \tag{2}$$

3.2 Equation of motion

This section introduces the equation of motion for the mechanical system. It is assumed that the mass of each link is located at the center of the link and each axis has a viscosity and elasticity associated with it. The equation of motion is then given by Eq. (3). $G(\theta)$ represents the gravitational force and it is assumed to be zero for side-to-side motion. $M(\theta) \in R^{N \times N}$ represents the inertia matrix which is a function of the joint angles. D_θ is the coefficient matrix for viscous friction and K_θ is the coefficient matrix for elasticity. $F = \tau / r$ represents the tension force, where τ is the motor torque and r is the radius of the pulley connected to the motor output. The coefficient matrix $E \in R^N$ expresses the effect of F on each joint. Now, we assume that F is evenly distributed along τ_{axis}. Then, the equation $\tau_{axis} = r_a / N \cdot F$ is derived, where r_a is the radius of each axis. Furthermore, the equation $E = r_a / N \cdot [1, 1, 1, \cdots, 1]^T$ is derived. Fig.7 shows an example for the case when $N = 5$.

$$ M(\theta)\ddot{\theta} + D_\theta \dot{\theta} + K_\theta \theta + G(\theta) = \tau_{axis} - \tau_{dis} \tag{3}$$

Where, $\tau_{axis} = [\tau_1, \tau_2, \cdots, \tau_N]^T = E \cdot F$,
$\tau_{dis} = [\tau_{dis,1}, \tau_{dis,2}, \cdots, \tau_{dis,N}]^T$,
$D_\theta = diag(D_1, D_2, D_3, \cdots, D_N)$,
$K_\theta = diag(K_1, K_2, K_3, \ldots, K_N)$,

4. CONTROLLER DESIGN

4.1 Controller design of sum of angles

The presented mechanical system driven by wires is an underactuated system since it has fewer actuators than the number of degrees of freedom. Therefore, it is not possible to control all of the angles using a linear control scheme such as the pole assignment method[11].

This paper describes the two steps of controller design. In the first step, for each direction separately, we design a sum of angles controller that makes $\theta_{sum} = \sum_{i=1}^{N} \theta_i$ track to the desired value θ_{sum}_r. In the second step, we design an image-based visual feedback control system on the exterior

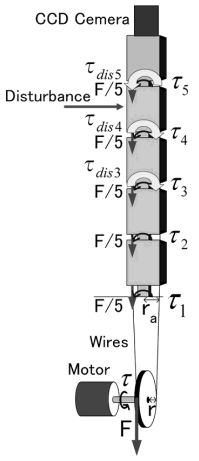

Fig. 7. Mechanism structure of apical part

of the sum of angles control system[3, 4, 5, 6]. First, the sum of angles is determined by multiplying the joint angle vector θ by the matrix $[1, 1, \cdots, 1]$ from the left. Fig.8 shows a block diagram of the transfer function from the tension F to $\dot{\theta}_{sum}$. Further, Fig.9 shows a block diagram of the visual feedback control system. In the diagram, the "System" block represents the content of Fig.8.

In the next step, this method described in this study utilizes the Lyapunov function to evaluate the stability of the sum of angles control system. To simplify the problem, τ_{dis} in Eq.(3) is neglected. Eq.(7) is solved using a simple PD control law and additional decoupling input.

$$F = K_p e_\theta - K_v \dot{\theta}_{sum} + \delta^{-1}(\zeta_1 \dot{\theta} + \zeta_2 \theta + \zeta_3 G(\theta)) \quad (4)$$

$$\begin{aligned} M(\theta)\,\ddot{\theta} + D_\theta \dot{\theta} + K_\theta \theta + G(\theta) &= E \cdot F \\ &= E\{K_p e_\theta - K_v \dot{\theta}_{sum} + \delta^{-1}(\zeta_1 \dot{\theta} + \zeta_2 \theta + \zeta_3 G(\theta))\} \end{aligned} \quad (5)$$

$$\begin{aligned} \ddot{\theta} &= -M^{-1}(\theta)\{D_\theta \dot{\theta} + K_\theta \theta + G(\theta)\} \\ &+ M^{-1}(\theta)[1,1,1,1,1]^T r_a/N \cdot F \end{aligned} \quad (6)$$

$$\ddot{\theta}_{sum} = [1,1,1,1,1]\ddot{\theta} = \delta(K_p e_\theta - K_v \dot{\theta}_{sum}) \quad (7)$$

Where, $e_\theta = \theta_r - \theta_{sum}, \dot{\theta}_r = 0$,
$\delta = [1,1,1,1,1]M^{-1}(\theta)[1,1,1,1,1]^T \cdot r_a/N$,
$\zeta_1 = [1,1,1,1,1]M^{-1}(\theta)D_\theta$,
$\zeta_2 = [1,1,1,1,1]M^{-1}(\theta)K_\theta$,
$\zeta_3 = [1,1,1,1,1]M^{-1}(\theta)$,

Assuming a candidate Lyapunov function given by Eq.(8), and making use of Eq.(7), its time derivative is expressed by Eq.(9).

$$V = \frac{1}{2}\delta^{-1} \cdot \dot{\theta}_{sum}^2 + \frac{1}{2} K_p e_\theta^2 \quad (8)$$

$$\begin{aligned} \dot{V} &= \delta^{-1}\dot{\theta}_{sum}\ddot{\theta}_{sum} + \frac{1}{2}\frac{d}{dt}(\delta^{-1})\dot{\theta}_{sum}^2 - K_p e_\theta \dot{\theta}_{sum} \\ &= -\{K_v - \frac{1}{2}\frac{d}{dt}(\delta^{-1})\}\dot{\theta}_{sum}^2 \end{aligned} \quad (9)$$

If $K_p > 0, \delta > 0$, then $V > 0$, except when $e_\theta = 0, \dot{\theta}_{sum} = 0$, and if we select a large $K_v (> 0)$, the result $\dot{V} < 0$ holds

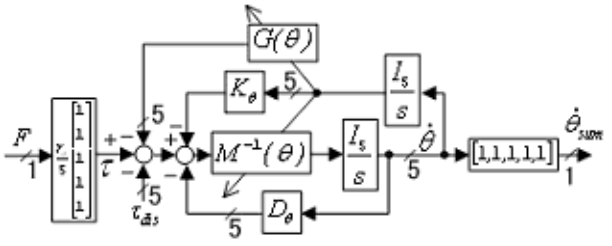

Fig. 8. Block diagram of the $\dot{\theta}_{sum}$ output system

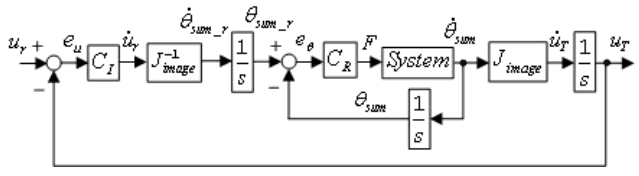

Fig. 9. Block diagram of visual feedback control system

for $\dot{\theta}_{sum} \neq 0$. Therefore, V becomes a Lyapunov function. Further, $\theta_{sum} \to \theta_r, \dot{\theta}_{sum} \to 0$ are performed.

4.2 Visual feedback controller design

This section describes the design method for the image-based visual feedback control system. We first need to determine the image Jacobian number. However, it is difficult to derive the components $f(\theta), g(\theta)$ of J_{sum}. Therefore, J_{image}, which is the ratio of $\dot{u}$ and $\dot{\theta}_{sum}$, is calculated using only Eq.(10).

$$J_{image} = \frac{\dot{u}}{\dot{\theta}_{sum}} \quad (10)$$

where $\dot{u}, \dot{\theta}_{sum}, J_{image} \in R$. This calculation of J_{image} is performed by substituting $\dot{u}, \dot{\theta}_{sum}$ for Eq. (10) during experiments in real time. Furthermore, the former value is utilized when $\dot{\theta}_{sum} = 0$. Next, the inverse value of J_{image} is substituted into the block "J^{-1}_{image}" shown in Fig.9. In this figure, $\dot{u}_r$ is expressed by Eq.(11).

$$\dot{u}_r = K_p(u_r - u_T) - K_v \dot{u}_T \quad (11)$$

These calculations are performed for every sampling period, and the value of θ_{sum_r} is continuously updated in real time.

5. EXPERIMENTAL RESULTS

This section introduces the experimental results that confirm the effectiveness of the control method presented above. Table1 indicates the physical parameters of the system, Table2,3 indicate the control parameters, and Fig.10 shows the experimental results for the side-to-side and up-and-down motions under the 20s time cyclic sinusoidal position disturbance by the disturbance stage. In this experiment, the disturbance stage generates four kinds of waves, which have time periods of $5, 10, 20$,and 40 s. Fig.11 shows a comparison of maximum errors of the target position on the screen. The results denoted "Constant Jaco" refer to the results obtained when the nominal Jacobian values are kept constant. And the results denoted "Updated Jaco" refer to the results obtained when the Jacobian values are updated in the manner described above. Fig.11(a) demonstrates that the presented control method is effective for disturbances having a period of longer than 20s . Fig.11(b) shows the case when gravity compensation was applied, but it appears to have no observable effect.

Table 1. Physical parameters

Number of links N	5
Mass of link m_i $(i = 1, 2, 3, 4)$	6.02×10^{-3} (kg)
Mass of link m_5	169.8×10^{-3} (kg)
Length of each link L_i $(i = 1, 2, 3, 4)$	2.0×10^{-2} (m)
Length of link L_5	7.5×10^{-2} (m)
Resolution of potentiometer $d\theta_p$	1.43 (V/rad)
Range of angles	$\pm 20 \times \pi/180$ (rad)
Radius of pulley r_i $(i = 1, 2, 3, 4)$	1.0×10^{-2} (m)
Radius of pulley r_5	3.75×10^{-2} (m)
Radius of axis r_a	7.5×10^{-3} (m)
Moment of inertia J_{rotor}	$6.77 \times 10^{-6} (kgm^2)$
Resolution of rotary encoder dE	$2\pi/3600$ (rad/pulse)

Table 2. Control parameters for side-to-side motion

Gain of stage controller K_{sd}, K_{sp}@	0.4 (NEs/m), 5.5 (N/m)
Sampling rate of stage controller	1.0 (ms)
Gain of joint controller K_{jd}, K_{jp}@	0.33 (NEs/rad), 5.61 (N/rad)
Sampling rate of joint controller	1.0 (ms)
Gain of visual feedback controller K_{vd}, K_{vp}@	1.32 (pixel · s /pixel), 3.96 (pixel/pixel)
Sampling rate of visual feedback	30 (ms)

Table 3. Control parameters for up-and-down motion

Gain of stage controller K_{sp}, K_{sd}@	1.5 (NEs/m), 6.3 (N/m)
Sampling rate of stage control	1.0 (ms)
Gain of joint controller K_{jd}, K_{jp}@	1.32 (NEs/rad), 3.63 (N/rad)
Sampling rate of joint controller	1.0 (ms)
Gain of visual feedback controller K_{vd}, K_{vp}@	0.66 (pixel · s /pixel), 8.58 (pixel/pixel)
Sampling rate of visual feedback	32 (ms)

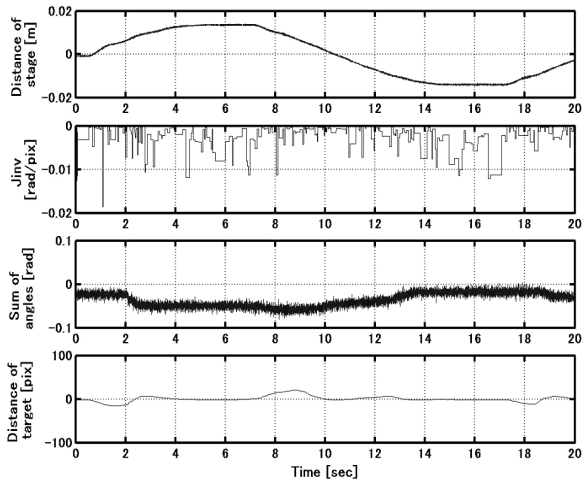

(a) side-to-side motion

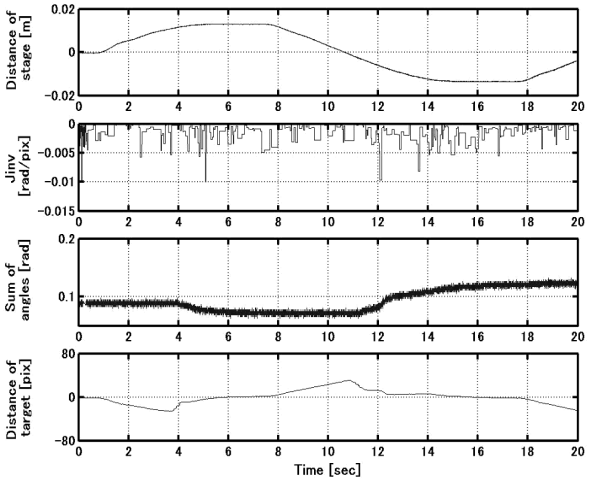

(b) up-and-down motion

Fig. 10. Experimental results for visual feedback control

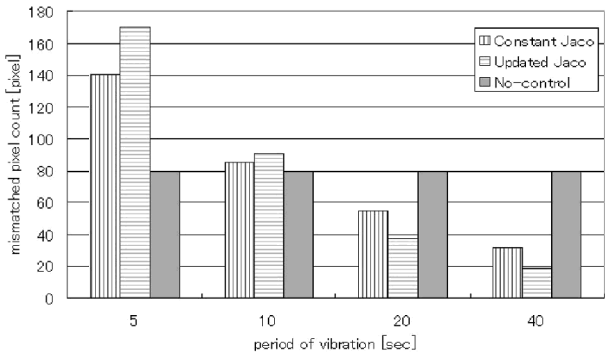

(a) side-to-side motion

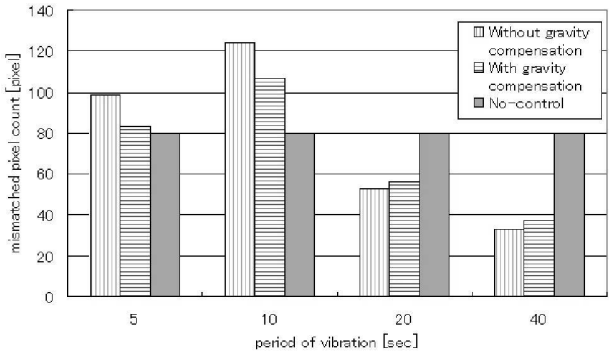

(b) up-and-down motion

Fig. 11. Experimental results for visual feedback control

Figs.12 (a) and (b) show sequential photographs of the motions. They show that the motion converges to the origin of the screen despite the application of force disturbances to the links.

6. CONCLUSION

This paper describes the controller design process of a visual feedback control system for a multiple degree of freedom system driven by wires with free joints and presents the experimental results obtained. These results demonstrate that the presented control system performs its intended function. However, the control performance is not sufficiently good. We therefore intend to continue to study this technique with the aim of improving it.

REFERENCES

[1] M.Higashimori, M.Kaneko, M.Ishikawa: Dynamic Preshaping for a Robot Driven by a Single Wire, 2003 IEEE International Conference on Robotics and Automation, pp.1115-1120, 2003

[2] K.Gotoh, A.Shimada: Visual Feedback Control of a Passive Redundant System, IEEJ Technical Meeting, IIC-07-30, 2007 (in Japanese)

[3] L.E.Weiss, A.C.Sanderson, C.P.Newman: Dynamic sensor-based control of robots with visual feedback, *IEEE J. Robotics and Automation*, Vol.RA-3, No.5, 1987, pp.404-417

[4] P.I. Corke: Visual control of robot manipulators - a review. In K.Hashimoto, editor, Visual Servoing, pp.1-32, World Scientific, Singapore, 1993

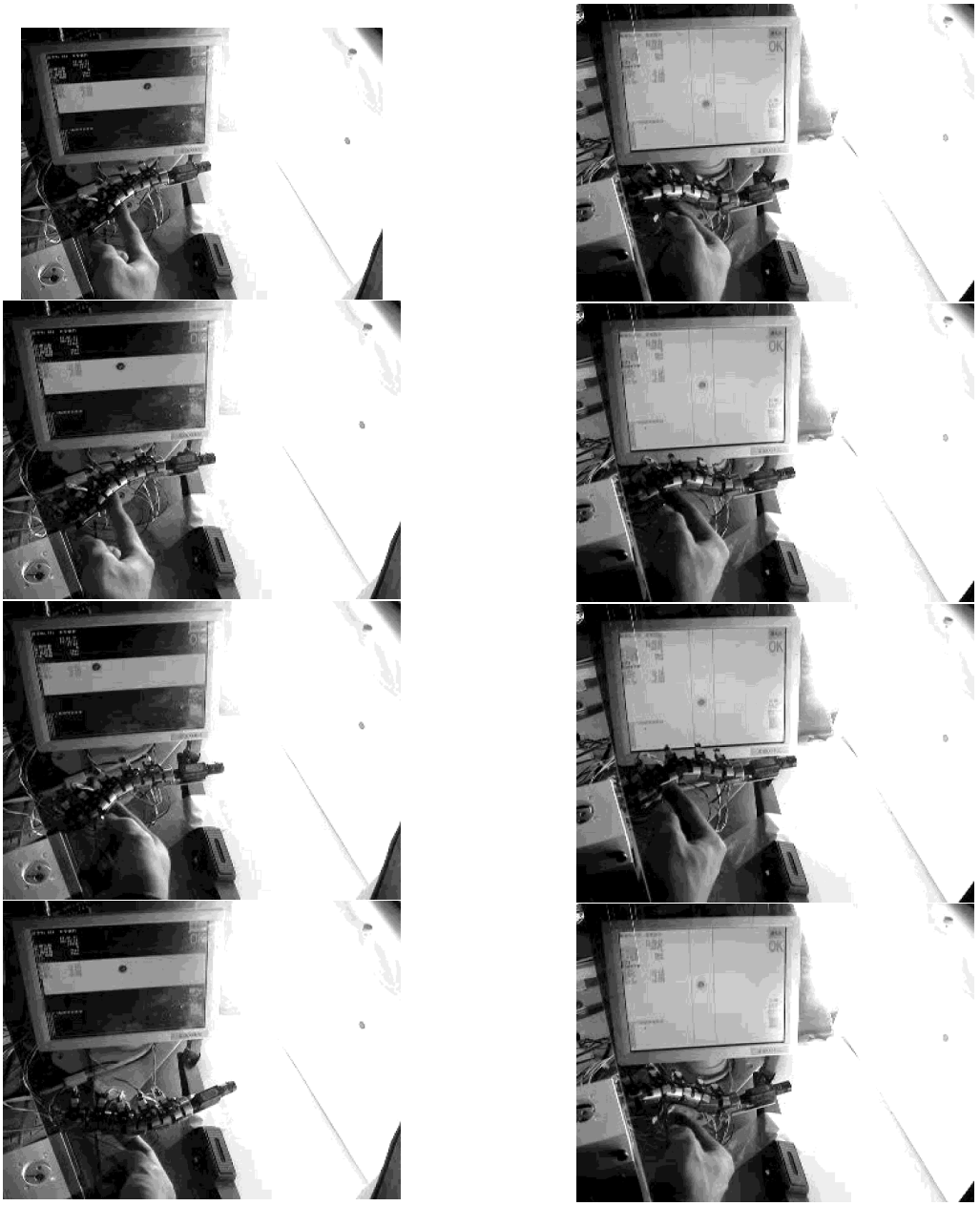

(a) side to side motion with force disturbance

(b) Up-and-down motion with force disturbance

Fig. 12. Photographs of the experiments

[5] S.Hutchinson, G.D.Hager, P.I.Corke: A tutorial on visual servo control, Trans. on Robotics and Automation, Vol.12, No.5, pp.651-670, 1996
[6] K.Hashimoto: Visual Servoing, J.SICE, Vol.35, No.4, pp.282-285, 1996 (in Japanese)
[7] Shigeo Hirose; Biologically Inspired Robots (Snake-like Locomotor and Manipulator), Oxford University Press(1993)
[8] K.Ikuta, M.Tsukamoto, S.Hirose, Shape Memory Alloy Servo Actuator System with Electric Resistance Feedback and its Application to Active Endoscope, Proc. of IEEE International Conference on Robotics and Automation, pp.427-430, 1988
[9] Y.Nakamura, M.Koinuma, T.Suzuki: Chaotic Behavior and Nonlinear Control of a Two-joint Planer Arm with a Free Joint, J. of RSJ, Vol.14, No.4, pp.602-611, 1996 (in Japanese)
[10] H.Arai, K.Tanie, N.Shiroma: Time-scaling Control of an Underactuated Manipulator, J.RSJ, Vol.16, No.4, pp.561-568, 1998 (in Japanese)
[11] R.W. Brockett: Asymptotic stability and feedback stabilization, in Differential Geometric Control Theory, Birkhauser, pp.181-208, 1983
[12] Tutomu Mita: Introduction to non-linear control theory, Shoko-do, 2000 (in Japanese)
[13] A.Shimada, N.Hatakeyama: High Speed Movement Control Making Use of Zero Dynamics on Inverted Pendulums, Trans. of SICE, Vol.42, No.9, pp.1035-1041, 2006 (in Japanese)